NONDESTRUCTIVE EVALUATION OF THERMAL BARRIER COATINGS BY MID-INFRARED REFLECTANCE IMAGING

Jeffrey I. Eldridge, Charles M. Spuckler, and James A. Nesbitt
NASA Glenn Research Center
21000 Brookpark Rd.
Cleveland, OH 44135

Richard E. Martin
Cleveland State University
Cleveland, OH

ABSTRACT

The application of mid-infrared reflectance (MIR) imaging to monitor damage in thermal barrier coatings (TBCs) has been extended from a previously demonstrated area-averaged spectroscopic analysis tool to become a practical imaging tool that provides the spatial resolution needed to quickly identify localized regions of TBC damage by visual inspection. Illumination optics and image collection procedures were developed to produce illumination-normalized flatfield reflectance images after subtraction of the background thermal emission. MIR reflectance images were collected with a bandpass filter centered at a wavelength of 4 microns, which provided the optimum balance between good sensitivity to buried cracks and coating erosion, but with a desirable insensitivity to TBC sintering and absorption from ambient gases. Examples are presented of the application of MIR reflectance imaging to monitor damage progression in plasma-sprayed 8wt% yttria-stabilized zirconia (8YSZ) TBCs subjected to either furnace cycling or alumina particle jet erosion. These results show that MIR reflectance imaging can reliably track the progression of buried delamination cracks produced by thermal cycling and can also be used to determine when any local section of the TBC has eroded beyond an acceptable limit. Modeling of the effects of buried cracks and erosion on reflectance will be presented to show the dependence of damage sensitivity to TBC thickness.

INTRODUCTION

Reliable diagnostic tools are needed to identify the location and severity of degradation in thermal barrier coatings (TBCs) on turbine engine components so as to provide adequate warning of when damage is approaching performance- or safety-threatening thresholds. Previous work has demonstrated that mid-infrared (MIR) reflectance spectroscopy exhibits a useful sensitivity to both TBC erosion and delamination progression, and has the particular advantage over many other diagnostic methods in exhibiting a sensitivity to the early stages of debond progression that enables early warning of subsequent spallation.[1] MIR reflectance spectroscopy takes advantage of the maximum transparency of TBCs in the 3-5 μm wavelength region,[2] allowing much greater penetration into the TBC than at visible wavelengths to detect the progress of the buried TBC delamination crack network that ultimately produces TBC failure. However, as previously implemented,[1] MIR reflectance spectroscopy was unsuitable for practical TBC health monitoring because these measurements averaged over large areas (20.6 mm diameter), precluding the detection of highly localized damage. In addition, measurements were restricted to small laboratory specimens that could be inserted into the spectrometer

enclosure. As presented in this paper, these limitations have been overcome by applying MIR reflectance as an imaging technique that provides a practical, easily interpreted health monitoring tool using visual inspection with the spatial resolution to identify localized damage.

EXPERIMENTAL PROCEDURES

MIR Reflectance Imaging

All images were obtained with a Phoenix (Indigo Systems, Santa Barbara) MIR camera with a LN_2 cooled 320x256 indium antimonide (InSb) focal plane array. A narrow 4.0 μm wavelength bandpass filter (FWHM=0.15 μm) was mounted on the camera because this wavelength offers good damage sensitivity while being sufficiently distant from potentially interfering OH and CO_2 absorptions at 3 and 4.25 μm, respectively. The camera was positioned 120 mm from the specimen. MIR illumination was provided by a SiC IR emitter operated at 50 W. The illumination from the source was collimated with a 63.5 mm diameter off-axis parabolic mirror that illuminated the specimens without shadowing by the source or loss of intensity with distance. It is important to note that while the off-axis parabolic mirror provides collimated, reproducible illumination, the illumination intensity is non-uniform; the intensity of the beam is higher where it reflects from areas of the mirror closer to the source. In order to improve signal to noise, each image represents an average of 800 frames captured at 30 Hz rate. Additionally, a detector integration time of 4.5 ms was employed for each frame to maximize signal level.

A sequence of image processing steps was performed to produce a true MIR reflectance image. These steps are necessary because the untreated image, $I_{raw\ image}$, includes background thermal radiation emitted by the specimen as well as illumination and pixel-to-pixel sensitivity variations:

$$I_{raw\ image}(x,y) = S(x,y)[I_0(x,y)R_{specimen}(x,y) + I_{thermal}(x,y)] \tag{1}$$

where x and y are the image coordinates, $S(x,y)$ is the individual pixel sensitivity, $I_0(x,y)$ is the position-dependent field-of-view illumination intensity, $R_{specimen}(x,y)$ is the specimen reflectance, and $I_{thermal}(x,y)$ is the thermal radiation emitted by the specimen. The thermal radiation term in Eq. 1 is eliminated by subtracting the image obtained with the illumination off, $I_{image}^{no\ illumination}(x,y) = S(x,y)I_{thermal}(x,y)$, from the image obtained with the illumination on:

$$\begin{aligned} I_{reflectance\ image}(x,y) &= I_{raw\ image}(x,y) - I_{image}^{no\ illumination}(x,y) \\ &= S(x,y)I_0(x,y)R_{specimen}(x,y) \end{aligned} \tag{2}$$

A flatfield correction is then made to remove the dependence on illumination and pixel-to-pixel variations. This is performed by normalizing to a reflectance image, $I_{standard}(x,y)$, collected from a 250 μm thick TBC standard with known reflectance, $R_{standard}(x,y)=R_{standard}=0.703$, that fills the field of view; this normalization produces an image where the pixel intensity is equal to the specimen reflectance:

$$\begin{aligned} I_{reflectance\ image}^{normalized}(x,y) &= \frac{I_{reflectance\ image}(x,y)}{I_{standard}(x,y)} R_{standard} \\ &= \frac{S(x,y)I_0(x,y)R_{specimen}(x,y)}{S(x,y)I_0(x,y)R_{standard}} R_{standard} = R_{specimen}(x,y) \end{aligned} \tag{3}$$

Specimen Preparation

The TBC specimens were prepared by atmospheric plasma-spraying a top coat of 8wt% yttria-stabilized zirconia (8YSZ) onto 25.4 mm diameter Rene N5 superalloy disks that were precoated with a ~120 μm-thick NiCrAlY bond coat by low pressure plasma-spraying. Selected samples were also produced for which the bond coat was applied to only half of the substrate top surface before the 8YSZ top coat deposition. In addition, freestanding plasma-sprayed 8YSZ (PS-8YSZ) TBCs were produced by spraying onto sacrificial carbon substrates that were later heat treated in air at 800°C to burn off the carbon. All as-deposited TBCs were heat treated for 3 min at 800°C to eliminate residual oxygen deficiencies that produce a grayish coloration in the as-sprayed specimens.

Furnace cycling tests were performed in a tube furnace in air, with each cycle consisting of a 45-min hold at 1163°C followed by a 15-min cooling period to ~120°C. After initial interrupted furnace cycling tests established TBC failure (buckled or spalled areas exceeding 20% of total TBC area) occurring at ~200 cycles, furnace cycling of three specimens was halted at different stopping points, specifically at 50, 100, and 150 cycles (¼, ½, and ¾ of cyclic life). MIR reflectance images were collected for these specimens, and SEM examination of prepared TBC cross-sections was performed. Controlled erosion was performed using a Koehler (Bohemia, NY) K93700 Air Jet Erosion Tester with a 5-mm-diameter nozzle using 50-μm-diameter alumina powder impinging on the specimen at an angle of 30° off normal.

RESULTS

The basis for using MIR reflectance to monitor TBC erosion is the decrease in MIR reflectance that accompanies reduction in TBC thickness. The ability to discriminate TBC thickness is shown clearly in MIR reflectance images (all images obtained with 4-μm-wavelength bandpass filter) of a wide range of freestanding TBC thicknesses ranging from 86 to 873 μm (Fig. 1). The MIR reflectance images in Fig. 1 are shown in two formats that display the specimen reflectance obtained through image processing (Equations 1-3) either in a conventional grayscale image or a 3-D intensity plot. Taking advantage of the spatial resolution provided by MIR reflectance imaging, the demonstrated thickness dependence of MIR reflectance can be utilized to identify highly localized eroded regions. Fig. 2 displays MIR reflectance images of 150 μm thick TBC specimens subjected to 1 and 2 min of localized alumina jet erosion. The eroded regions are evident by their lower reflectance due to the reduced TBC thickness caused by the erosion.

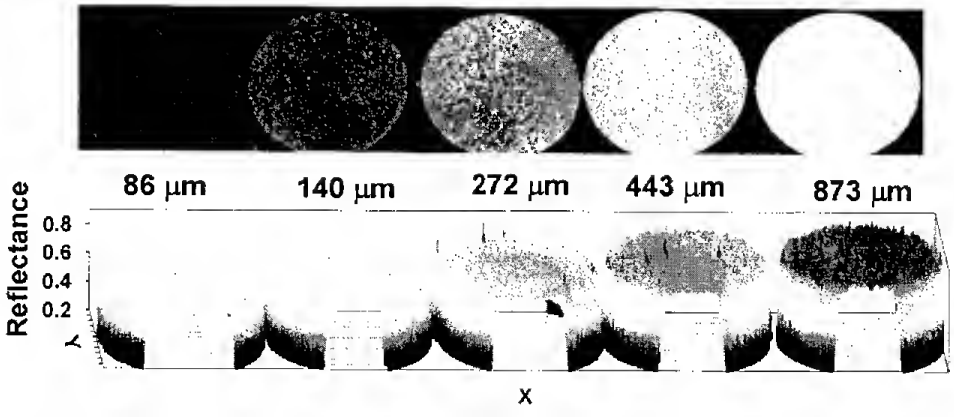

Figure 1. Thickness dependence of MIR reflectance images of freestanding 8YSZ TBCs. (Top) Grayscale reflectance image. (Bottom) 3-D Reflectance intensity plot.

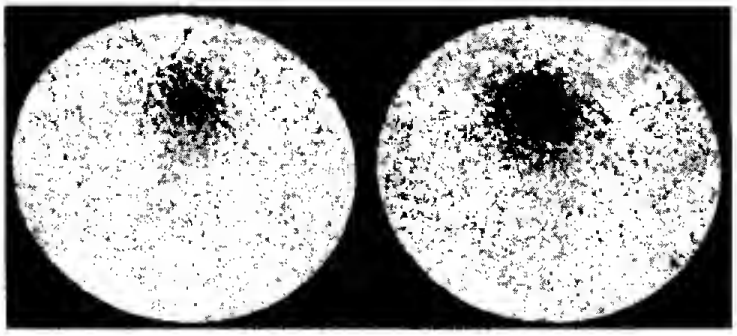

Figure 2. MIR reflectance images of 150-μm-thick TBC-coated specimens after 1 min (left) and 2 min (right) of local alumina particle jet erosion.

MIR reflectance imaging can also be used to monitor the TBC delamination. To demonstrate the spatial resolution of the imaging approach and to determine the range of thicknesses over which the progress of TBC delamination could be distinguished, MIR reflectance images were acquired from freestanding TBCs that had been backside-coated over half their back surfaces (half-backed) with 2-μm-thick NiAl by sputter deposition to mimic an adherent substrate (the unbacked half mimics a delaminated TBC). Because no heat treatment was applied to produce "delamination", any differences in MIR reflectance could be attributed to the presence or absence of the adherent backside NiAl coating. Fig. 3 shows a sequence of 73, 125, and 295 μm thick half-backed TBCs that show a significantly lower reflectance over the well-defined half-backed section for the two thinner TBCs, with the reflectance difference decreasing with increased TBC thickness until the contrast is only barely discernable at 295 μm thickness. These results indicate MIR reflectance should be capable of discerning TBC delamination with good spatial resolution, but with decreasing contrast as the TBC thickness increases.

Fig. 4 demonstrates that MIR reflectance imaging can also monitor the actual delamination progression associated with furnace cycling of TBC-coated substrates. Fig. 4 compares MIR reflectance images of 175-μm thick TBC-coated specimens after 0, 50, 100, 150, and 200 furnace cycles (visible buckling was observed at 200 cycles). There is a continuous increase in reflectance at 4-μm wavelength from 0.56 to 0.75 that is associated with failure progression, while there are no noticeable reflectance differences under visible light illumination. SEM inspection (Fig. 5) of the cross-sections of the same furnace-cycled specimens confirmed a TBC failure progression similar to that observed in previous studies:[3] the formation and growth of a delamination crack network along the bottom of the TBC, mostly above the thermally grown oxide (TGO) that grows on top of the bond coat. Backscatter electron detection provided superior contrast for cracks compared to secondary electron detection. Fig. 5 shows that the crack network grows by lengthening and widening of individual cracks as well as increasing crack interconnectedness. While TGO growth also occurs, very little TGO growth was observed after 50 cycles (average TGO thickness was 4.6, 4.5, and 5.6 μm thick at 50, 100, and 150 cycles, respectively).

Because delamination progression proceeded uniformly over the surfaces of the furnace-cycled specimens imaged in Fig. 4, another set of specimens was prepared where the bond coat was applied to only half of the substrate top surface before the 8YSZ top coat deposition. Because TBCs without bond coats fail much earlier and with a higher degree of scatter than

TBCs with bond coats,[1] these test specimens were imaged to demonstrate spatially resolved monitoring of localized delamination. Fig. 6 shows MIR reflectance images of one 175-μm-thick 8YSZ-coated specimen after 0, 10, 20, and 30 furnace cycles. The left half of the specimen has a bond coat while the right half does not. While the bond coat half shows a uniform increase in reflectance (consistent with Fig. 4), the no-bond-coat half shows both a greater increase in overall reflectance along with localized bright regions that grow from the edge that eventually evolve into visible edge-initiated delamination.

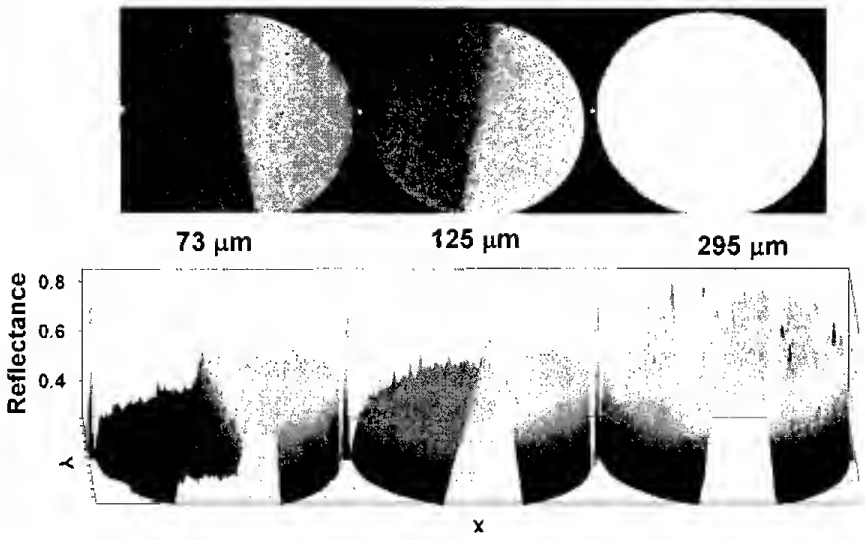

Figure 3. MIR reflectance images of freestanding 73, 125, and 295 μm thick 8YSZ TBCs with backside half-coated with NiAl to mimic adherent substrate. NiAl backside coating is on left half of each image. (Top) Grayscale reflectance image. (Bottom) 3-D Reflectance intensity plot.

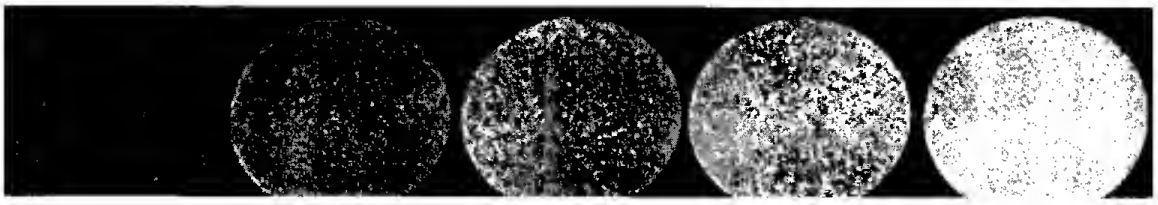

0 cycles	50 cycles	100 cycles	150 cycles	200 cycles
R=0.56	R=0.65	R=0.68	R=0.71	R=0.75

Figure 4. MIR reflectance grayscale images of 175-μm-thick 8YSZ TBC-coated specimens after 0, 50, 100, 150, and 200 furnace cycles. Average reflectance for each specimen is also indicated. Visible TBC buckling was observed at 200 cycles.

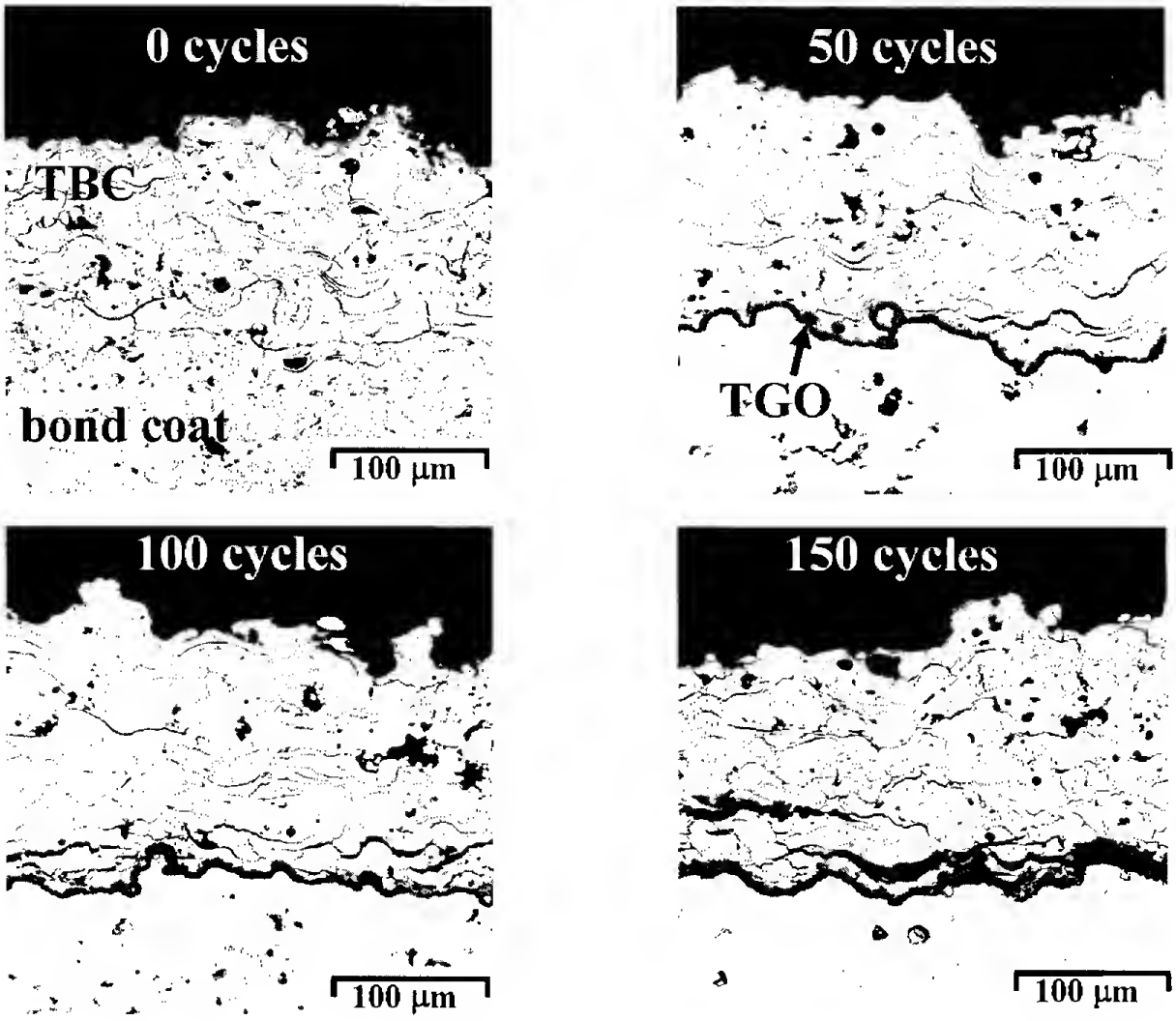

Figure 5. Backscatter electron images of cross-sections of 175-μm-thick 8YSZ TBC-coated specimens after 0, 50, 100, and 150 furnace cycles.

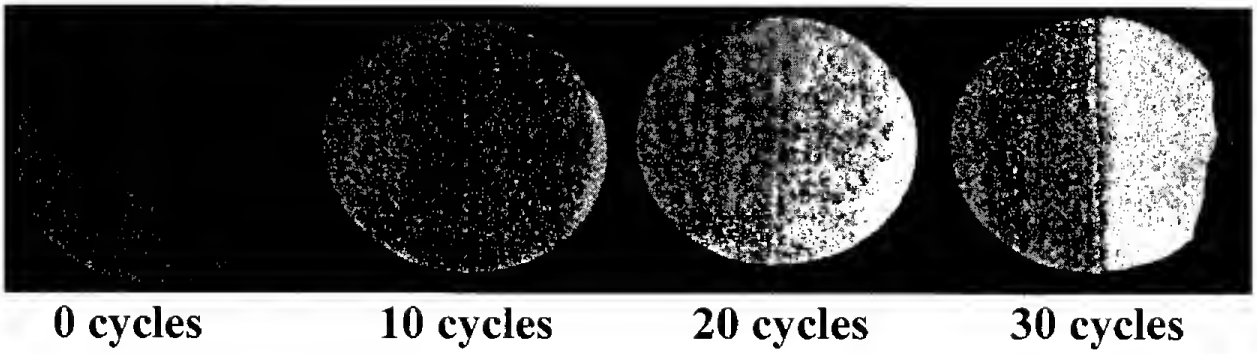

Figure 6. MIR reflectance grayscale images of the same 175-μm-thick 8YSZ TBC-coated specimen after 0, 10, 20, and 30 furnace cycles. Bond coat was applied only to left half of specimen before 8YSZ top coat deposition.

DISCUSSION

The ability of MIR reflectance imaging to map regions of TBC erosion or partial delamination relies both on the deep penetration of MIR wavelengths into the TBC as well as the contrast-producing mechanisms produced by changes in TBC thickness or the introduction of buried cracks. In order to predict the range of TBC thicknesses over which reductions in TBC thickness or delamination could be discerned from MIR reflectance, a four-flux Kulbelka-Munk approximation[4] was applied to the extreme cases of a completely adherent and a completely detached TBC. The detached TBC was modeled simply by a uniform air gap between the TBC and the substrate. In this model, the substrate (bond coat) was assigned a diffuse reflectance of 0.43, and calculations predicted the introduction of an air gap produces a very high diffuse reflectance of 0.81 at the TBC/air gap interface due to a large component of total internal reflection arising from the large index of refraction change across that interface (from n=2.1 to n=1.0). The scattering and absorption coefficients for the plasma-sprayed 8YSZ TBCs at a wavelength of 4 μm were determined to be 359 and 0.035 cm^{-1}, respectively (calculated from reflectance/transmittance vs. thickness measurements from a series of freestanding TBCs). The predicted effect of introducing the air gap on the reflectance at 4 μm wavelength as a function of TBC thickness is plotted in Fig. 7. This plot has important implications for the range of TBC thicknesses where MIR reflectance will be useful for monitoring erosion or delamination. First, the reflectance curve for the attached TBC shows less sensitivity to changes in TBC thickness as TBC thickness increases. Secondly, the difference (which produces the contrast) in reflectance between an adherent and completely detached TBC decreases with increasing TBC thickness, and it can be concluded that MIR reflectance will not be useful for either erosion or delamination monitoring for TBCs thicker than 500 μm. Two experimental points (at 0 and 200 cycles, representing attached and detached, respectively) have been added to Fig. 7, illustrating good agreement with the prediction. These calculations ignore the potential effect of TGO growth on reflectance; however, the expected parabolic TGO growth results in a decreasing growth rate, and the TGO growth measurements indicate little growth beyond 50 cycles. Therefore, the TGO growth would only have a significant effect on the increase in reflectance observed during the early stages of furnace cycling. It should also be noted that these results are for plasma-sprayed TBCs and that MIR reflectance may prove useful up to much greater thicknesses for electron-beam physical vapor deposited (EB-PVD) coatings, which have much lower scattering coefficients.

In summary, MIR reflectance imaging has been developed along with the image processing required to remove the thermal radiation emitted by the specimen and fluctuations due to nonuniform illumination and pixel-to-pixel sensitivity variation. This imaging approach provides a practical, easily interpreted health monitoring tool using visual inspection with the spatial resolution to identify localized damage from erosion and the ability to predict the onset and location of TBC delamination. MIR reflectance imaging shows excellent potential as a diagnostic tool for investigating TBC failure progression in the laboratory, and also shows potential for between-flight engine inspections for TBC erosion and early-stage delamination in environments where surface fouling does not occur.

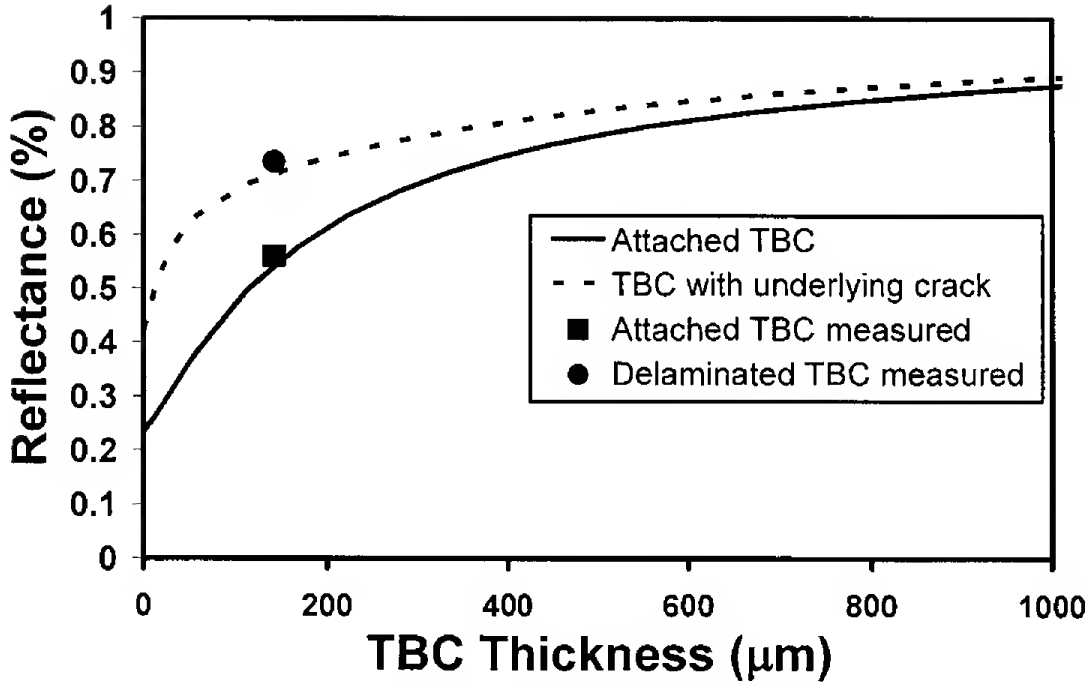

Figure 7. Predicted effect of introduction of crack (gap) at plasma-sprayed 8YSZ TBC/substrate interface on reflectance at 4.0 μm wavelength as a function of TBC thickness. Measured reflectance values are also included for a TBC specimen after 0 cycles (attached) and 200 cycles (delaminated).

ACKNOWLEDGMENTS

The authors wish to thank George Leissler, Sandy Leissler, and Gary Kostyak for coating deposition, Richard Mondry for erosion testing, Chuck Barrett for furnace cycling, and Luke Hertert for assistance in developing the image acquisition software.

REFERENCES

[1]J.I. Eldridge, C.M. Spuckler, J.A. Nesbitt, and K.W. Street, "Health Monitoring of Thermal Barrier Coatings by Mid-Infrared Reflectance," *Ceram. Eng. Sci. Proc.*, **24**[3], 511-16 (2003).

[2]J.I. Eldridge, C.M. Spuckler, K.W. Street, and J.R. Markham, "Infrared Radiative Properties of Yttria-Stabilized Zirconia," *Ceram. Eng. Sci. Proc.*, **23**[4], 417-30 (2002).

[3]J.T. DeMasi-Marcin, K.D. Sheffler, and S. Bose, "Mechanisms of Degradation and Failure in a Plasma-Deposited Thermal Barrier Coating," ASME J. Eng. Gas Turbines and Power, **112**, 521-26 (1990).

[4] T. Makino, T. Kunitomo, I. Sakai, and H. Kinoshita, "Thermal Radiation Properties of Ceramic Materials," *Heat Transfer – Jpn. Res.*, **13**[4], 33-50 (1984).